

# Understanding ferromagnetism in Co-doped TiO<sub>2</sub> anatase from first principles

Rebecca Janisch\* and Nicola A. Spaldin

Materials Department, University of California, Santa Barbara, California 93106, USA

(Received 9 September 2005; revised manuscript received 11 November 2005; published 3 January 2006)

We present a first-principles computational study of the nature and origin of ferromagnetism in Co-doped TiO<sub>2</sub>. We calculate the magnetic ordering and electronic properties as a function of the concentration and distribution of Co dopants and oxygen vacancies. We find that Co atoms prefer to substitute on neighboring sites of the Ti lattice, and show, using the well-established Goodenough-Kanamori-Anderson rules, that this leads to a ferromagnetic superexchange. We propose other semiconductor hosts in which the superexchange mechanism should lead to ferromagnetic coupling between the magnetic moments of neighboring transition metal dopants.

DOI: [10.1103/PhysRevB.73.035201](https://doi.org/10.1103/PhysRevB.73.035201)

PACS number(s): 75.50.Pp, 61.72.Ji

## I. INTRODUCTION

In the rapidly growing research field known as “spintronics” there is nowadays considerable interest in the design of dilute magnetic semiconductors, with a particular focus on the exploration of different semiconductor hosts. Among these, Co-doped TiO<sub>2</sub> has attracted much attention. In particular, the first report of robust, room-temperature ferromagnetism by Matsumoto *et al.*,<sup>1</sup> generated tremendous interest in its potential as a dilute magnetic semiconductor (DMS) for device applications. Subsequent experimental studies have yielded ferromagnetic Curie temperatures ( $T_C$ 's) up to ~650 K. However, a large spread of  $T_C$ 's and magnetizations continue to be reported, depending on the preparation conditions, the resulting oxygen content of the samples and the distribution and concentration of Co (for a review see Ref. 2). A consensus on the origin of the experimentally observed ferromagnetic coupling has not yet been reached.

In this work we perform a detailed computational study of Co-doped TiO<sub>2</sub>, with the goal of identifying the origin of ferromagnetism, and determining the effects of various material parameters on the magnetic behavior. Specifically, we calculate the magnetic ordering and electronic properties, as a function of Co concentration, and distribution, and oxygen vacancy concentration and distribution. The advantage of such a computational study is that these different influences, which occur simultaneously in an experimental sample, can be studied independently.

The main result of our work is that, when Ti ions are substituted by Co ions in anatase TiO<sub>2</sub>, the lowest energy magnetic configuration is indeed the ferromagnetic one. Therefore it is plausible that, at least in some cases, the experimental reports of ferromagnetism result from true substitutional DMS behavior, rather than from Co precipitates. Furthermore, we can provide an explanation for the origin of this ferromagnetism in terms of a combination of kinetic energy lowering in half-metallic samples and ferromagnetic superexchange in insulating samples or regions.

## II. COMPUTATIONAL METHOD

We performed *ab initio* total-energy and electronic-structure calculations using the ABINIT density functional

theory code<sup>3</sup> within the local spin density approximation<sup>4</sup> (LSDA). The LSDA is a widely used approximation for the exchange-correlation functional in density functional theory (DFT),<sup>5</sup> which is very successful in predicting many material properties. However, it also has some well-known shortcomings: Energies of excited states, and in particular band gaps in semiconductors, are systematically underestimated, binding is overestimated so that bond lengths are too small and bandwidths are too broad, and in magnetic systems the LSDA often predicts a metallic, low-spin state of magnetic ions, for systems which are experimentally insulating and high-spin. Therefore, in addition to our LSDA calculations, we cross-check our results using a successful “beyond-LSDA” method; the pseudopotential self-interaction corrected (pseudo-SIC) method developed by Filippetti *et al.*<sup>6</sup> In this approach, the spurious interaction of the electron with its own Coulomb and exchange-correlation potential, which is present within the LSDA, is subtracted within a pseudopotential framework yielding results for magnetic systems that are in better agreement with experiment than those of the LSDA.<sup>6</sup> The pseudo-SIC gives similar results to the more widely used LDA+ $U$  method,<sup>7</sup> but without the difficulty of selecting a value for  $U$ .

### A. Technical details

Both the ABINIT and pseudo-SIC codes are plane-wave pseudopotential implementations, in which the wave functions are expanded in a basis of plane waves, and the valence electron-ion interaction is represented by a pseudopotential. For our ABINIT LSDA (pseudo-SIC) calculations we used Teter type extended norm-conserving (Vanderbilt type ultrasoft) pseudopotentials, with valence configurations  $3s^2, 3p^6, 4s^2, 3d^2$  for Ti,  $3s^2, 3p^6, 4s^2, 3d^7$  for Co, and  $2s^2, 2p^4$  for O.

In both cases we perform scalar relativistic calculations, i.e., in the following the term “magnetic moment” does not denote a vector quantity, but simply a local inequality in the filling of up-spin and down-spin electronic states. Thus it is not possible to make any statements about the orientation of the magnetization or about effects of spin-orbit coupling.

As a result of the highly localized Co  $d$  states, the total energy calculations for Co-doped TiO<sub>2</sub> are unusually techni-

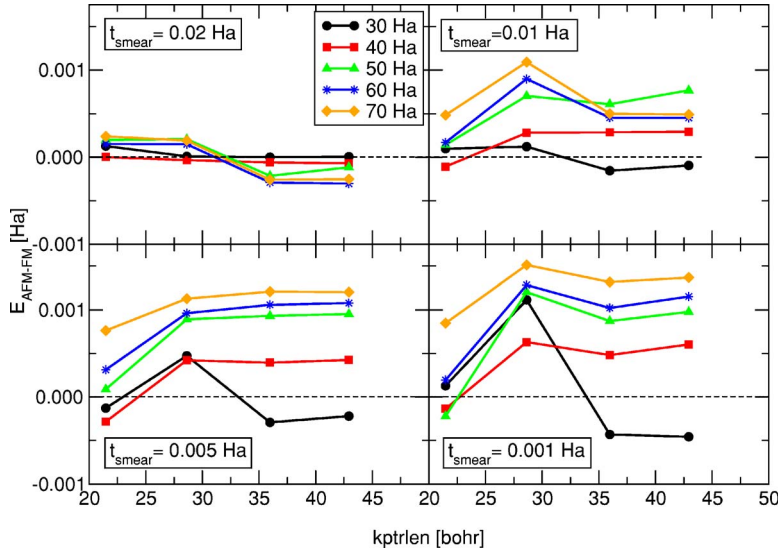


FIG. 1. (Color online) Convergence behavior of the energy difference between antiferromagnetic and ferromagnetic alignment of the Co magnetic moments in  $\text{Co}_2\text{Ti}_2\text{O}_8$ . Shown is  $E_{AFM-FM}$ , the difference in total energies for antiferromagnetic and ferromagnetic alignment of the Co magnetic moments vs “kptrlen,” the length of the smallest real space unit vector of the Fourier-transformed  $k$ -point mesh, which is a measure of the  $k$ -point density. The different graphs show results for different smearing factors  $t_{\text{smear}}$  of the Gaussian smearing scheme, each for a set of different cut off energies of the plane-wave basis set, ranging from 30 to 70 hartree.

cally demanding. First, they are difficult to converge, and second, poorly converged calculations often give qualitatively incorrect results. For example, a calculation in which the  $k$ -point sampling or the plane wave energy cutoff is too small, can predict the wrong magnetic ground state. Therefore, here we describe the convergence behavior in some detail. We hope that this section will shed some light on the unusually large inconsistencies among some computational results in the literature.

To check the convergence of the energy difference between ferromagnetic and antiferromagnetic alignment of the moments,  $E_{AFM-FM} = E_{AFM}^{tot} - E_{FM}^{tot}$ , we used a 12-atom unit cell with the experimental lattice parameters of  $\text{TiO}_2$  anatase, and two of the four Ti atoms substituted by Co. In Fig. 1 we show the calculated LSDA energy difference as a function of the following three parameters.

(a) The density of the  $k$ -point mesh, represented in the figure by the length of the smallest real space unit vector of the Fourier transformed  $k$ -point mesh [labeled kptrlen (bohr)].

(b) The cut off energy of the plane-wave basis set (in Ha).

(c) The temperature factor which broadens the occupation numbers in the metallic cases, labeled  $t_{\text{smear}}$  (Ha) in the figure. Each energy level is broadened by a factor  $e^{-x^2/\sqrt{\pi}}$ , where  $x$  is the energy divided by  $t_{\text{smear}}$ .

It can be seen that at high smearing factors magnetic effects are more or less “smeared out,” independent of the density of the  $k$ -point mesh. For  $t_{\text{smear}} = 0.02$  Ha the energy difference for the highest cutoffs is only around  $2.5 \times 10^{-4}$  Ha ( $\approx 6.8$  meV  $\approx 80$  K). With decreasing  $t_{\text{smear}}$   $E_{AFM-FM}$  becomes larger, and sufficient convergence is reached at  $t_{\text{smear}} \leq 0.005$  Ha, for kptrlen  $\geq 35$  bohr (for the 12 atom unit cell this corresponds to a  $6 \times 6 \times 3$   $k$ -point mesh) and  $E_{\text{cut}} \geq 50$  Ha. The LSDA results which are presented in the following were obtained using the latter set of convergence parameters. (In the pseudo-SIC calculations the energy cut-off could be reduced to 20 Ha, due to the use of ultrasoft pseudopotentials.)

We point out, also, that accurate geometry optimization around the substituted ions is essential to obtain meaningful

results. We relaxed the atomic positions until the remaining forces were smaller than  $10^{-4}$  Ha/bohr.

### III. RESULTS

#### A. LSDA

We started with a 12-atom  $\text{TiO}_2$  unit cell, optimized the cell parameters and relaxed the internal coordinates. The cell parameters were calculated to be  $a_0 = 3.79$  Å, and  $c/a = 2.51$ , with the internal displacement parameter  $u = 0.208$ . These structural parameters are in excellent agreement with experimental data (see, e.g., Ref. 8). The total density of states is shown in Fig. 2. We see that the band gap, separating the largely oxygen  $2p$  valence band from the largely Ti  $3d$  conduction band, is  $\approx 2.2$  eV in the LSDA, consistent with the results of earlier computational studies employing both the LSDA (Ref. 9) and generalized gradient approximation (GGA).<sup>10</sup> The result also shows the typical underestimation of the gap compared to the experimental value of 3.2 eV (see, e.g., Ref. 11).

Next, we studied the electronic properties in the dilute limit, by constructing a 48-atom  $2 \times 2 \times 1$  supercell of the conventional  $\text{TiO}_2$  anatase unit cell (Fig. 3) and substituting one Ti atom by Co. This yields a dopant concentration of 6.25 at. %.

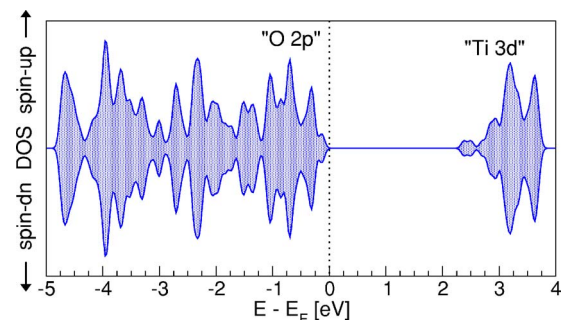


FIG. 2. (Color online) Total density of states for pure  $\text{TiO}_2$  anatase. The band gap of the pure crystal is  $\approx 2.2$  eV in the LDA.

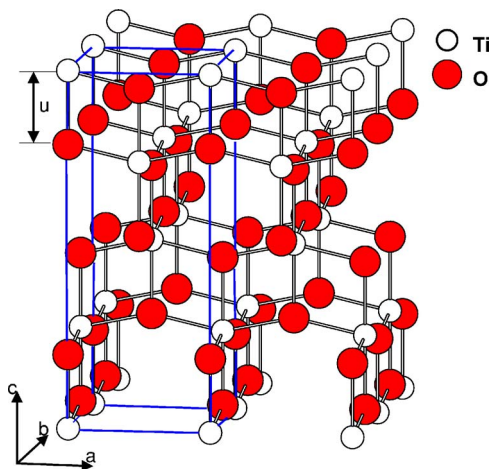


FIG. 3. (Color online)  $2 \times 2 \times 1$  anatase supercell. The conventional body-centered-tetragonal unit cell which contains four formula units is indicated by straight lines

Keeping the volume fixed at the calculated equilibrium volume for the pure cell, we relaxed all internal atomic coordinates. Around the Co atom the internal displacement parameter  $u$  is reduced to 0.193 (from 0.208), i.e., the oxygen atoms relax towards Co. Using these atomic positions, we then calculated the electronic properties; the density of states is shown in Fig. 4(a). The pure  $\text{TiO}_2$  band gap of 2.2 eV can still be identified, with Co impurity states lying well isolated in the gap. The magnetic moment of the supercell is  $1 \mu_B$ , suggesting that Co adopts a low-spin,  $(t_{2g}^\uparrow)^3(t_{2g}^\downarrow)^2$  state; this can also be seen clearly in the density of states plot and is in agreement with the results of previous works (Refs. 9, 10, 12, and 13).

The simple molecular orbital diagram for a  $\text{Co}(\text{O})_6$  octahedral cluster [Fig. 4(b)] is helpful in interpreting the calculated density of states. The irreducible representations of the 3d, 4s, and 4p states of the transition metal ( $t_{2g}$ ,  $e_g$ ,  $a_{1g}$ , and  $t_{1u}$ ) interact with the corresponding oxygen 2p ( $t_{1u}$ ,  $t_{1g}$ ,  $t_{2u}$ , and  $t_{2g}$ ) and 2s ( $a_{1g}$ ,  $e_g$ , and  $t_{1u}$ ) irreducible representations, to form the bonding and antibonding molecular orbitals shown in the central panel (spin splittings are neglected in the diagram). Electron counting then reveals that the up-spin Co-derived antibonding  $t_{2g}^*$  states are fully occupied, and that the Fermi energy lies within the down-spin  $t_{2g}^*$  manifold. In Fig. 4(c) the molecular orbital diagram is aligned with the LSDA DOS to highlight the comparison.

For comparison the density of states (DOS) for the “test cell” used for the convergence tests (also with fully relaxed internal parameters) is shown in Fig. 5. Due to the high concentration of Co (25 at. %) the original  $\text{TiO}_2$  gap is now filled with impurity states. However, we clearly see a spin splitting, leading to a half-metallic DOS, even if the gap in the majority states is very small. The magnetic moment per Co atom in this case is again 1 bohr magneton, corresponding to the low-spin state of Co. Thus we can conclude that the spin-state of Co is independent of the Co concentration up to very high concentrations. This is in agreement with the earlier findings of Errico *et al.*<sup>13,14</sup> for Co in rutile-structure  $\text{TiO}_2$ .

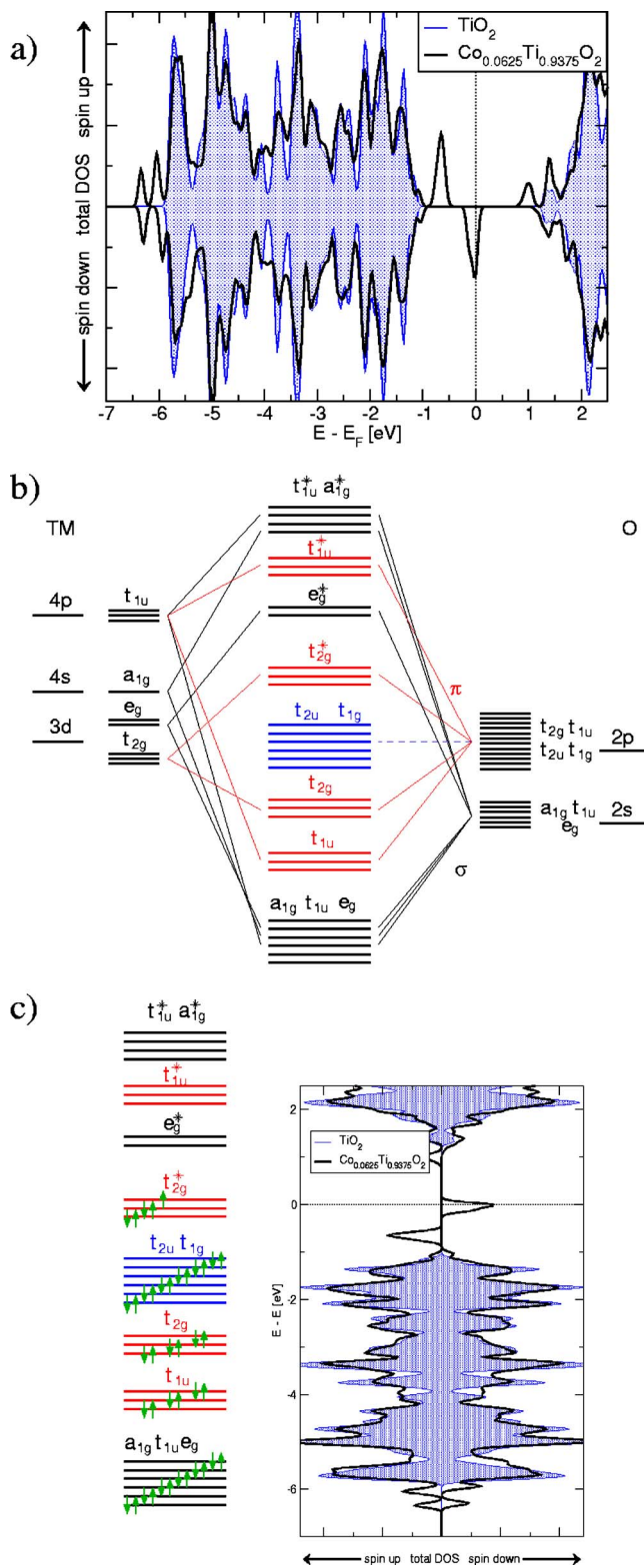
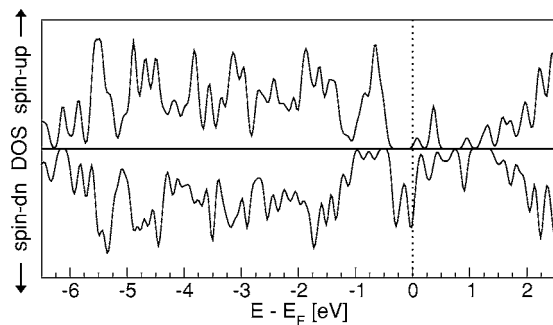


FIG. 4. (Color online) (a) Total density of states for pure  $\text{TiO}_2$  anatase (shaded plot; color online) and  $\text{Co}_{0.0625}\text{Ti}_{0.9375}\text{O}_2$ . The band gap of the pure crystal does not change significantly upon doping. (b) Molecular orbital scheme for a three-dimensional (3D)-metal atom in an octahedral oxygen complex. (c) Comparison of (a) and (b) shows that in  $\text{Co}_{0.0625}\text{Ti}_{0.9375}\text{O}_2$  the Fermi level lies in the antibonding Co  $t_{2g}^*$  states.

FIG. 5. Total density of states for  $\text{Co}_{0.25}\text{Ti}_{0.75}\text{O}_2$ .

Introducing a vacancy in the oxygen octahedron surrounding the Co atom (and relaxing the atomic positions) does not change the total magnetic moment of the supercell either. We can see from Fig. 6(a) that the main effect of the oxygen vacancy is the lifting of the octahedral symmetry on the Co site and therefore a splitting of the Co  $d$  peaks in the band gap. However, the relative occupation of spin-up and spin-down states, and thus the magnetic moment remains the same. Figure 6(b) shows the DOS for the same system, but with the oxygen vacancy shifted by one lattice vector  $\mathbf{a}$ . In contrast, in this case the oxygen octahedron around Co is left intact (apart from slight changes due to relaxations of the atomic positions in the whole supercell) and the DOS resembles that of the vacancy-free  $\text{Co}_{0.0625}\text{Ti}_{0.9375}\text{O}_2$  cell. However, the Co  $t_{2g}$  states are almost filled now, and the magnetic moment is reduced to  $0.13\mu_B/\text{Co}$ . The first case, in which the two defects are close to each other, is the more favorable one, a trend which fits with the observations of Jaffe *et al.*<sup>15</sup> Their results also show that although the magnitude of the local moments does not increase in the presence of oxygen vacancies, the spin-spin interaction is enhanced.

Next, we substituted a second Co atom in the 48-atom supercell, giving a Co concentration of 12.5 at. %

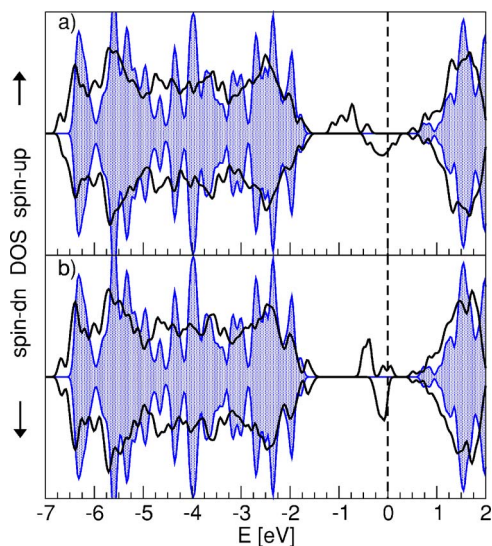


FIG. 6. (Color online) Total density of states of Co-doped  $\text{TiO}_{2-\delta}$ . (a)  $\text{CoTi}_{15}\text{O}_{31}\square$  with the oxygen vacancy next to the Co atom. (b)  $\text{CoTi}_{15}\text{O}_{31}\square$  with the oxygen vacancy shifted by one lattice vector  $\mathbf{a}$ .

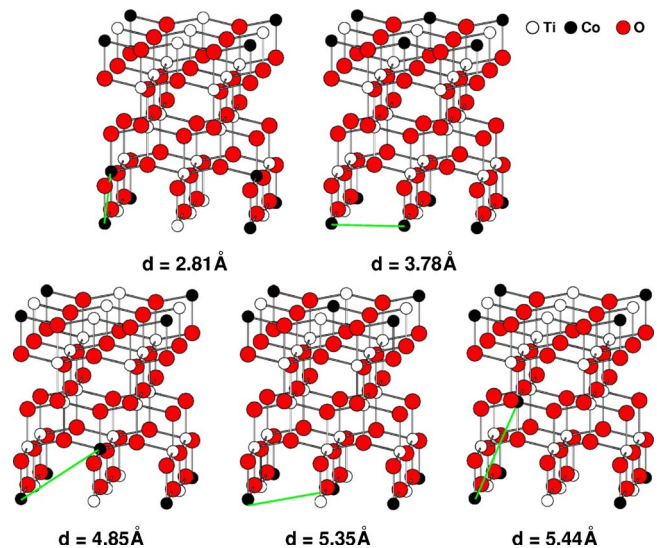


FIG. 7. (Color online) Co-doped  $\text{TiO}_2$  anatase cells with 12.5 at. % Co.

( $\text{Co}_{0.125}\text{Ti}_{0.875}\text{O}_2$ ), and allowing us to evaluate the relative energies of ferro- and antiferromagnetically ordered states. We varied the positions of the Co atoms, to investigate the tendency of Co to cluster and to test the dependency of the magnetic coupling on interatomic distance, bond angles, and coordination. Our choice of unit cell allows five different relative Co-Co positions, as shown in Fig. 7. Again, the internal coordinates were relaxed for each arrangement, while the volume of the supercell was kept fixed.

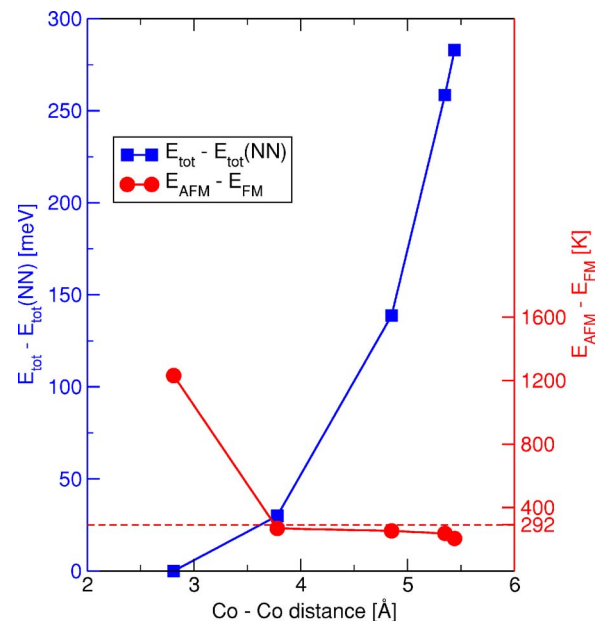


FIG. 8. (Color online) Left axis; Total energy of the different  $\text{Co}_{0.125}\text{Ti}_{0.875}\text{O}_2$  supercells shown in Fig. 7 relative to the nearest-neighbor configuration (squares), plotted versus the Co-Co distance. Right axis; Energy difference between antiferromagnetic and ferromagnetic alignment of the Co magnetic moments, normalized by the number of interacting Co-Co pairs (circles). The temperature equivalent ( $\Delta E \approx k_B T$ ) of this energy difference is also given, and the dashed line indicates room temperature.

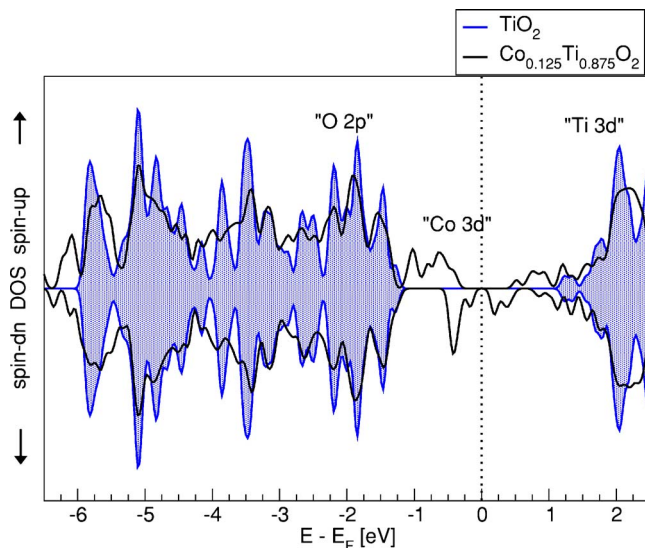


FIG. 9. (Color online) Density of states for the 48-atom supercell of Co doped  $\text{TiO}_2$  (12.5 at. % Co). In this case the Co atoms occupy nearest-neighbor positions on the Ti lattice. The electronic structure, shown for the case of parallel alignment of the Co magnetic moments, is insulating. The shaded plot represents the total DOS of the pure  $\text{TiO}_2$  cell.

We obtain four main results, which are relevant to our later discussion of the mechanism for ferromagnetism.

(i) For all arrangements, the ferromagnetic (FM) arrangement is lower in energy than the antiferromagnetic (AFM), with the energy difference  $E_{AFM-FM}$  largest ( $\approx 106$  meV per Co pair) for nearest-neighbor Co ions, then dropping off quickly with Co-Co separation.

(ii) The total energy of the supercell is lowest for the smallest Co-Co distance, i.e., for the Co atoms occupying nearest-neighbor positions on the metal sublattice. The energy then increases continuously with increasing distance, as shown in Fig. 8. This is consistent with earlier computations<sup>10,15</sup> and with the experimental tendency of Co ions to cluster together in practical samples.<sup>16,17</sup>

(iii) For all arrangements of the Co ions, we obtain a magnetic moment per Co atom of  $1\mu_B$ , as in the case of 6.25 at. % Co. This indicates again a low-spin configuration for the Co ions, independent of the Co concentrations, as observed by Errico *et al.* for Co-doped rutile.<sup>13,14</sup>

(iv) The electronic structure of the nearest-neighbor configuration is insulating, as illustrated by the density of states shown in Fig. 9. For more distant Co pairs, the material is half-metallic within the LSDA, as found in earlier calculations (using the LDA as well as the GGA, e.g., Refs. 9, 10, and 18). Interestingly, Errico *et al.*, who investigated rutile doped with different concentrations of Co found an insulating electronic structure for all cases considered within both the LDA and the GGA approximations.<sup>13,14</sup>

### B. Pseudo-SIC

Finally, we test the validity of the conclusions reached above from the LSDA calculations, by repeating selected calculations using the pseudo-SIC method. In particular, we check, for the 12 atom supercell with one Co atom (25 at. % doping), whether the low-spin state of Co persists within the pseudo-SIC (a high-spin state becomes more probable within beyond LDA methods), and whether the half-metallicity is lifted.

First, to compare structural predictions of the LDA and pseudo-SIC methods we calculated energy-volume curves for the pure  $\text{TiO}_2$  supercell at fixed  $c/a$  ratio. The equilibrium volumes and bulk moduli thus obtained differ by less than 1%. Therefore, we use our relaxed LDA structures for the pseudo-SIC calculations which follow. Figure 10 shows our calculated band structures of pure  $\text{TiO}_2$  anatase, within the LDA (left) and the pseudo-SIC (right) approximations. Although the two band structures are qualitatively very similar, we see that the pseudo-SIC energy gap (3.1 eV) is satisfyingly close to the experimental gap of 3.2 eV, whereas, as noted earlier, the LSDA gap shows the characteristic underestimation. The accurate band gap obtained by the pseudo-SIC ensures the correct placement of the impurity bands relative to the host band edges.

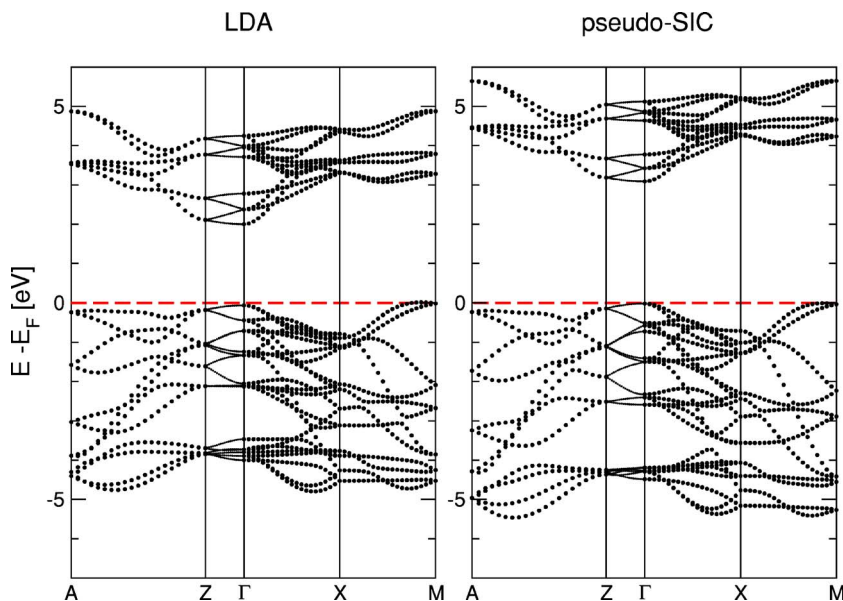


FIG. 10. (Color online) Band structure of pure  $\text{TiO}_2$  anatase, within the LDA (left) and the pseudo-SIC (right).

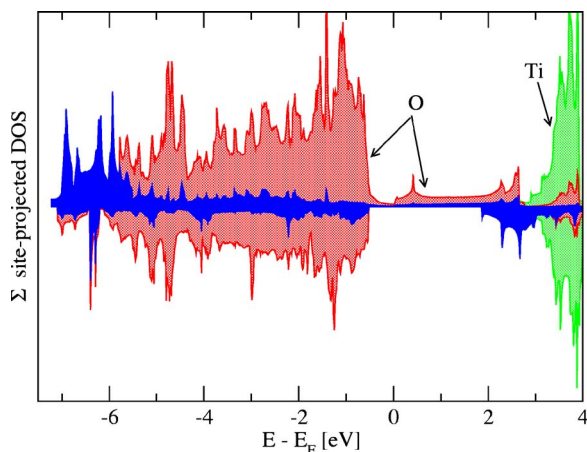


FIG. 11. (Color online) Density of states, calculated with application of the pseudo-SIC, site projected on the different atoms of the supercell and subsequently summed up for the different elements. Dark solid plot, Co; shaded plot, O, respectively, Ti.

When one Co ion is included in the 12-atom supercell ( $\text{CoTi}_3\text{O}_8$ ), the magnetic moment obtained within pseudo-SIC is 1 bohr magneton, as in the LSDA case. Therefore the lowspin state of Co persists within pseudo-SIC, and is indeed likely to be the true experimental configuration. In Fig. 11 we show the pseudo-SIC site-projected densities of states. It is clear that correcting the self-interaction results in a strong energy lowering of the occupied Co  $d$  states, which shift down into the valence band and become strongly hybridized with the oxygen  $p$  states. The pseudo-SIC system is close to insulating; A band structure calculation (not shown) reveals a single, highly dispersive, oxygen-derived band crossing the Fermi energy. In contrast, the LSDA system is strongly half-metallic. Such a gap opening is characteristic of beyond-LDA calculations for strongly correlated systems, and reinforces our conclusion that the electronic structure of the 12.5% doped material with nearest-neighbor Co ions is insulating. On the other hand, the half-metallicity predicted by the LSDA for other Co configurations will certainly be weakened in practice.

#### IV. DISCUSSION; ORIGIN OF FERROMAGNETISM

The origin of ferromagnetism in diluted magnetic semiconductors is often discussed in terms of a competition between short-ranged antiferromagnetic superexchange interactions, and long-ranged carrier-mediated mechanisms which promote ferromagnetic order.<sup>19</sup> Indeed in conventional, tetrahedrally-bonded semiconductors, such as GaAs or ZnO, this description is almost certainly appropriate. There are many situations, however, in which the superexchange mechanism can lead to *ferromagnetic* coupling between neighboring transition metal dopants.

Here we revisit the well-established Goodenough-Kanamori-Anderson (GKA) rules<sup>20–23</sup> to show that, in Co-doped  $\text{TiO}_2$  anatase, the superexchange mechanism indeed leads to ferromagnetic coupling between the magnetic moments of neighboring transition metal dopants. The sign and

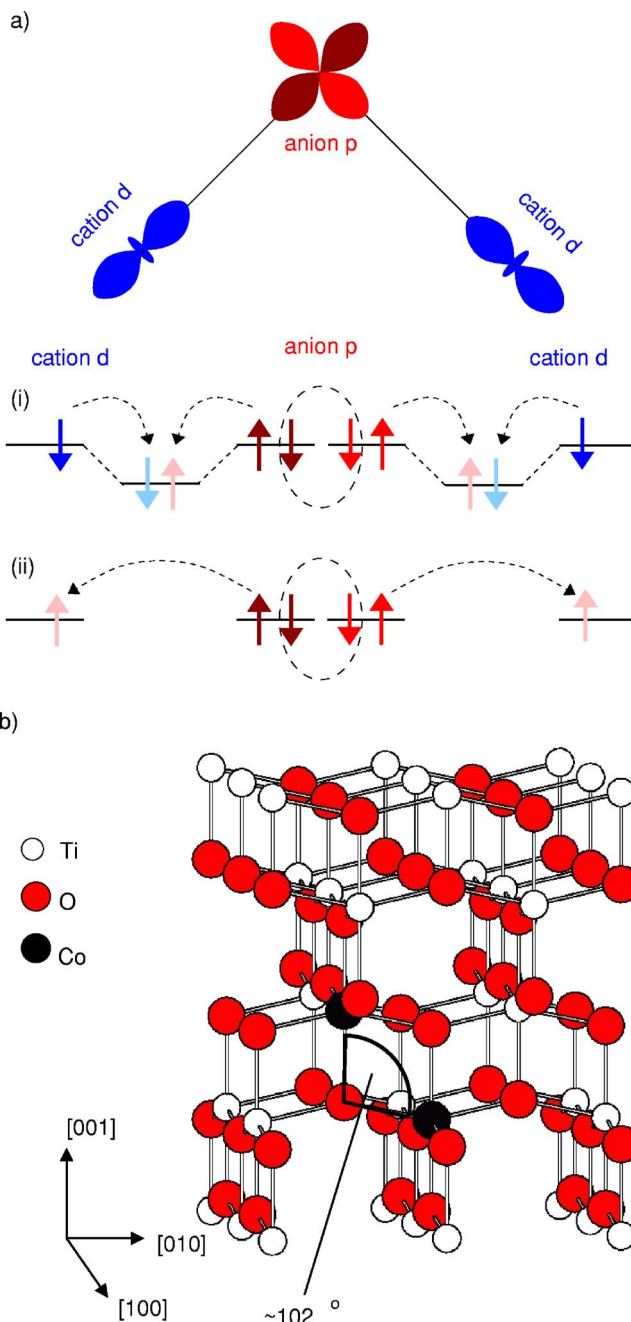


FIG. 12. (Color online) (a)  $90^\circ$  superexchange between identical transition metal cations. If the cation  $d$  orbitals are occupied (i), they interact with their neighboring anion  $p$  orbitals via covalent bond formation with the  $p$  electrons of opposite spin to their own. If the  $d$  orbitals are empty (ii), they accept electron density from their neighboring anion ligands; the anion electron's spin is parallel to that of the cation by Hund's first rule. In both cases, the non-bond-forming  $p$  electrons couple ferromagnetically to each other via direct exchange leading in both cases to ferromagnetic coupling between the metal ions. (b) Lowest energy configuration for 12.5 at. % Co in anatase  $\text{TiO}_2$ .

magnitude of the anion-mediated superexchange interaction between neighboring magnetic ions in transition metal salts is determined by the metal-anion-metal bond angle, the symmetry of the crystal field, and the  $d$  electron configuration of

the transition metal. Although accurate electronic structure calculations such as those described above are required to calculate the *magnitude* of the interaction, its sign can be predicted reliably using the simple GKA rules. Within this framework, the exchange interaction is regarded as being composed of two terms; kinetic exchange between the non-orthogonal orbitals of the participating atoms, the sign of which depends on the filling of the transition metal *d*-states, and potential exchange between orthogonal orbitals on the same atom, which is always ferromagnetic.

Figure 12(a) depicts the situation for a 90° metal-anion-metal bond; in all cases the superexchange between two like (i.e., same element and same oxidation state) transition metal ions is ferromagnetic. This is in sharp contrast to the antiferromagnetic superexchange obtained for 180° metal-anion-metal bonds between like ions. Therefore, in Co-doped TiO<sub>2</sub>, the local superexchange interaction between Co ions in their preferred structural configuration is ferromagnetic. As a consequence, the local magnetic interactions do not compete with the long-range carrier-mediated interactions in this material, since both are ferromagnetic. These observations are consistent with the robust, experimentally measured ferromagnetism in both insulating and conducting samples of Co-doped TiO<sub>2</sub>. Note that for spacings other than nearest-neighbor, the superexchange, although weak, is likely to revert to AFM, and will again be in competition with carrier-mediated FM exchange. More examples would be needed to

make a quantitative analysis of the different contributions.

Based on our analysis, we encourage the experimental exploration of semiconductor hosts containing 90° metal-anion-metal bonds as promising candidates for robust, high temperature ferromagnets. Although this geometry requirement excludes the conventional zincblende- and wurtzite-structure semiconductors, suitable hosts include spinel-type oxides (AB<sub>2</sub>O<sub>4</sub>) in which the B sites have *only* 90° interactions, as well as perovskites (such as BaTiO<sub>3</sub>), and materials with the sodium chloride, anatase, and rutile structures (such as MgO, TiO<sub>2</sub> and SnO<sub>2</sub>, respectively).

## V. SUMMARY

In summary, our electronic structure computations indicate that the lowest energy arrangement for substitutional Co in anatase TiO<sub>2</sub> occurs when the Co ions occupy neighboring Ti sites. The Co ions adopt low-spin electron configurations and order ferromagnetically. These results are robust to the choice of exchange-correlation functional used in the calculation. The clustering of the Co-dopants is energetically favorable because the energy of substitutional Co in TiO<sub>2</sub> anatase is rather high,<sup>9</sup> the ferromagnetic configuration is favored by the 90° superexchange interactions and/or half-metallicity.

\*Present address: Fakultät für Elektrotechnik und Informationstechnik, Professur für Opto- und Festkörperelektronik, Technische Universität Chemnitz, 09107 Chemnitz, BRD

<sup>1</sup>Y. Matsumoto, M. Murakami, T. Shono, T. Hasegawa, T. Fukumura, M. Kawasaki, P. Ahmet, T. Chikyow, S. Koshihara, and H. Koinuma, *Science* **291**, 854 (2001).

<sup>2</sup>R. Janisch, P. Gopal, and N. A. Spaldin, *J. Phys.: Condens. Matter* **17**, R657 (2005).

<sup>3</sup>X. Gonze, J.-M. Beuken, R. Caracas, F. Detraux, M. Fuchs, G.-M. Rignanese, L. Sindic, M. Verstraete, G. Zerah, F. Jollet, *et al.*, *Comput. Mater. Sci.* **25**, 478 (2002).

<sup>4</sup>W. Kohn and L. J. Sham, *Phys. Rev.* **140**, A1133 (1965).

<sup>5</sup>P. Hohenberg and W. Kohn, *Phys. Rev.* **136**, B864 (1964).

<sup>6</sup>A. Filippetti and N. A. Spaldin, *Phys. Rev. B* **67**, 125109 (2003).

<sup>7</sup>V. I. Anisimov, F. Aryasetiawan, and A. I. Lichtenstein, *J. Phys.: Condens. Matter* **9**, 767 (1997).

<sup>8</sup>M. Horn and C. F. Schwerdtfeger, *Z. Kristallogr.* **136**, 273 (1972).

<sup>9</sup>Z. Yang, G. Liu, and R. Wu, *Phys. Rev. B* **67**, 060402(R) (2003).

<sup>10</sup>W. T. Geng and K. Kim, *Solid State Commun.* **129**, 741 (2004).

<sup>11</sup>H. Tang, H. Berger, P. E. Schmid, and F. Lévy, *Solid State Commun.* **87**, 847 (1993).

<sup>12</sup>J. M. Sullivan and S. C. Erwin, *Phys. Rev. B* **67**, 144415 (2003).

<sup>13</sup>L. A. Errico, M. Weissmann, and M. Rentería, *Phys. Status Solidi B* **241**, 2399 (2004).

<sup>14</sup>L. A. Errico, M. Weissmann, and M. Rentería, *Physica B* **354**, 338 (2004).

<sup>15</sup>J. E. Jaffe, T. C. Droubay, and S. A. Chambers, *J. Appl. Phys.* **97**, 079308 (2005).

<sup>16</sup>D. H. Kim, J. S. Yang, K. W. Lee, S. D. Bu, T. W. Noh, S.-J. Oh, Y.-W. Kim, J.-S. Chung, H. Tanaka, H. Y. Lee, *et al.*, *Appl. Phys. Lett.* **81**, 2421 (2002).

<sup>17</sup>S. R. Shinde, S. B. Ogale, J. S. Higgins, H. Zheng, A. J. Millis, V. N. Kulkarni, R. Ramesh, R. L. Greene, and T. Venkatesan, *Phys. Rev. Lett.* **92**, 166601 (2004).

<sup>18</sup>M. S. Park, S. K. Kwon, and B. I. Min, *Phys. Rev. B* **65**, 161201(R) (2002).

<sup>19</sup>J. M. D. Coey, M. Venkatesan, and C. B. Fitzgerald, *Nat. Mater.* **4**, 173 (2005).

<sup>20</sup>P. W. Anderson, *Phys. Rev.* **79**, 350 (1950).

<sup>21</sup>J. B. Goodenough, *Phys. Rev.* **100**, 564 (1955).

<sup>22</sup>J. Kanamori, *J. Phys. Chem. Solids* **10**, 87 (1958).

<sup>23</sup>P. W. Anderson, in *Magnetism*, edited by G. T. Rado and H. Suhl (Academic Press, New York and London, 1963), Chap. 2, p. 25.